Automotive Science and Engineering, Vol. 11, No. 4, (2021),3693-3700

Iran University of Science and Technology

Automotive Science and Engineering

Journal Homepage: ase.iust.ac.ir

ISSN: 2717-2023

Chaotic Analysis and Chaos Control of a Lateral Dynamics Vehicle Based on the Nonlinear Poincaré Map with Fuzzy Controller

Farhad Pashaei[1], Seyed Mahdi Abtahi [2*]

[1]Department of Mechanical Engineering, Qazvin Branch, Islamic Azad University, Qazvin, Iran

[2]Department of Mechanical Engineering, Qazvin Branch, Islamic Azad University, Qazvin, Iran

ARTICLE INFO

Article history:
Received:3 Nov 2021
Accepted:9 Dec 2021
Published:30 Dec 2021

Keywords:
Chaos control
Fuzzy inference
Poincaré map
Vehicle lateral dynamics

A B S T R A C T

In this paper, firstly chaotic behavior of the lateral dynamics of vehicle is investigated by the use of numerical tools including Lyapunov exponent and bifurcation diagrams. To this end rout to chaos along with period doubling and quasi-periodic responses are demonstrated in terms of bifurcation diagrams. After chaos analysis, a novel controller commensurate with the chaotic characteristics of the system, in conformity with Poincaré map is represented to suppress the chaotic behavior of lateral movement. The Poincaré map of the system is derived by means of a neuro fuzzy network. A robust Fuzzy system on the basis of nonlinear Ott-Grebogi-Yorke (OGY) method forms the control system. Closed-loop results of the system shows effectiveness of the chaos controller in extreme conditions.

1. Introduction

Chaos control based on the characteristics of the chaotic system leads to generating a small control signal and less energy consumption. In 1990, [1] proposed a controller based on the characteristics of the chaotic system such that a pole placement method was used in accordance with the linear Poincaré map. Since then, OGY control principles were developed. Thus efficient control algorithms were implemented on the basis of linear or nonlinear Poincaré Map of the system resulting in fast convergence to the fixed points and stabilizing the orbits which are periodically unstable. In this method, the controller brings the system to equilibrium point with a small control signal which seems to be an advantage for the control system. [2]–[4].

In order to stabilize the lateral movements of the vehicle, active or differential steering, adaptive brakes or a combination of them are applied. Nevertheless the Active Front Steering controller can well increase vehicle stability and occupant comfort [5]–[6].

In terms of active chaos control of a vehicle, [7] presented an active controller based on the chaotic behavior generated by the nonlinear model characteristics of the MR dampers in a typical heavy articulated vehicle. In 2019, [8] suggested a controller based on adaptive sliding mode to suppress chaos in vehicle lateral movements, in which fuzzy logic was used to reduce errors.

In this paper, at first the vehicle dynamics is modeled. Then, in chaos analysis, Lyapunov exponential, and bifurcation diagrams are used to investigate different aspects of chaos in the system. In the controller design, an algorithm based on Poincaré map is implemented. Thus, to derive the Poincaré map, the appropriate Poincaré section is extracted and the map is determined by the use of neuro-fuzzy method. In this work Poincaré map is kept nonlinear and a robust fuzzy controller is determined. The results proof that the novel controller is efficient in controlling the chaos behavior of the system.

*Corresponding Author
Email Address: m.abtahi@qiau.ac.ir
https://doi.org/10.22068/ase.2021.602

[DOI: 10.22068/ase.2021.602]

2. Dynamical Modeling

In this paper, a nonlinear four-wheel drive vehicle model has been used. Nonlinear tire behavior, longitudinal and transverse movements due to vertical tire load, roll effects, Camber angle changes due to vehicle roll can be considered as nonlinear effects. The model includes nonlinear effects and roll movement in addition to the rotational dynamics of the wheels and steering mechanism. In this model, air resistance and pitch are ignored. Moreover, a constant longitudinal velocity is considered. Also, the axis of the roll is parallel to the horizontal plane and the effects between the roll and yaw are not taken into account. The effects of unsuspended weight are neglected. The nonlinear model of the vehicle is shown in Figure 1 [8].

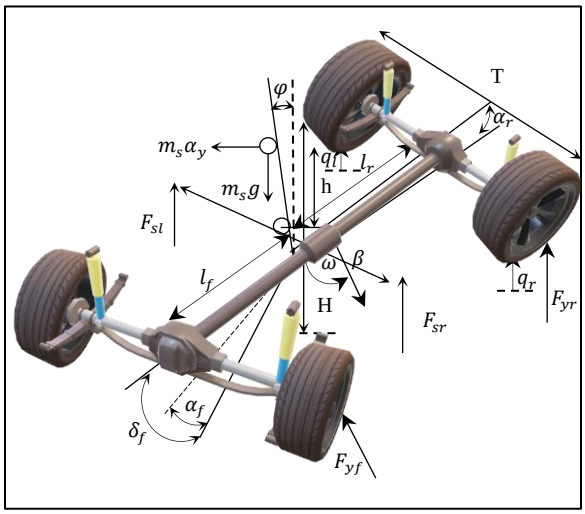

Figure 1. Schematic of Lateral, Yaw and Roll of the Vehicle

, where ω, β and φ are yaw, lateral angle and roll, respectively. The dynamic equations governing the vehicle, including lateral movements, yaw, and roll, are obtained using Newton-Euler method as follows [8]:

$$\begin{aligned} &I_z\dot{\omega} = 2l_fF_{yf}\cos\delta_f - 2l_rF_{yr} \\ &mv(\dot{\beta}+\omega) - m_sh\ddot{\varphi} = 2F_{yf}\cos\delta_f + 2F_{yr} \\ &(I_{sx}+m_sh^2)\ddot{\varphi} = m_sgh\varphi + m_shv(\dot{\beta}+\omega) \\ &\qquad + (T/2)F_{sl} - (T/2)F_{sr} \end{aligned} \quad (1)$$

To express the interactions between lateral and longitudinal forces of the tire, the Magic Formula for nonlinear tire model with combined longitudinal and lateral angles are used. The sideslip angles of the front and rear wheels are [8].

$$\begin{aligned} \alpha_f &= -\delta_f + tan^{-1}\left(\beta + (l_f\omega_r/v)\right) \\ \alpha_r &= tan^{-1}(\beta - (l_r\omega_r/v)) \end{aligned} \quad (2)$$

Here δ_f is angle of the front steering and v is the longitudinal speed of the vehicle. The vertical forces of the axes, without affecting their nonlinearity, are obtained to simplify the model based on the following equations [8]:

$$F_{yf} \approx C_f\alpha_f - C_{fl}\alpha_f^3 \, , F_{yr} \approx C_r\alpha_r - C_{rl}\alpha_r^3 \quad (3)$$

Where C_f and C_r show the linear stiffness of the front and rear wheels. C_{fl} and C_{rl} represent nonlinear stiffness. Also, for suspension system of the vehicle, which includes nonlinear effects such as springs and dampers, linear and nonlinear stiffness coefficients are used for the vibration properties of the suspension system [8]:

$$F_{si} = k_iz_i + k_{i2}z_i^3 + C_{si}\dot{z}_i + C_{i1}\dot{z}_i^3 \qquad i = l, r \quad (4)$$

The road surface input [8] is:

$$\dot{q}_i = -2\pi f_0q_i + 2\pi w_i\sqrt{G_0u} \quad i = l, r \quad (5)$$

, where G_0 and w_i are the road roughness coefficient and Gaussian white noise respectively. f_0 is the low-pass frequency and q_i is the distance from the road surface. Power spectral density and roughness exponents on average roads are applied to simulate the natural surface of the road [8]. Also, the road roughness coefficient and other parameters are listed in Table 1.

Table 1. Vehicle Model Parameters [8]

Parameter (Unit)	**Value**	**Parameter** (Unit)	**Value**
M (kg)	2832	**H** (m)	1.00
$\boldsymbol{m_s}$ $(\boldsymbol{kg})$	2592	**T** (m)	1.57
$\boldsymbol{I_z}$ $(\boldsymbol{kg.m^2})$	3488	$\boldsymbol{k_r, k_l}$ $(N.m^{-1})$	16000
$\boldsymbol{I_x}$ $(\boldsymbol{kg.m^2})$	2614	$\boldsymbol{C_{sl}, C_{sr}}$ $(N.s.m^{-1})$	5570
$\boldsymbol{l_f}$ $(\boldsymbol{m})$	1.26	$\boldsymbol{k_{r2}, k_{l2}}$ $(N.m^{-1})$	-1000
$\boldsymbol{l_r}$ $(\boldsymbol{m})$	1.7	$\boldsymbol{C_{l1}, C_{r1}}$ $(N.s.m^{-1})$	-360
h (m)	0.65	$\boldsymbol{G_0}$ $(\times 10^{-6}m^3/cycle)$	64

3. Chaos analysis

Front steering angle of the vehicle is determined by $\delta_f = A_0 \sin\omega_0 t$. Runge-Kutta method is used to solve the equations numerically. According to Figure 2-a chaotic behavior in roll angle is obvious. 3D-trajectories are presented in figures 2-b and 2-c.

[DOI: 10.22068/ase.2021.602]

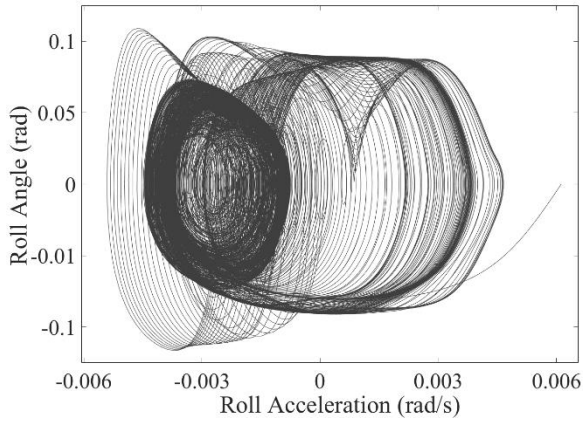

a. Trajectory of the Roll angle

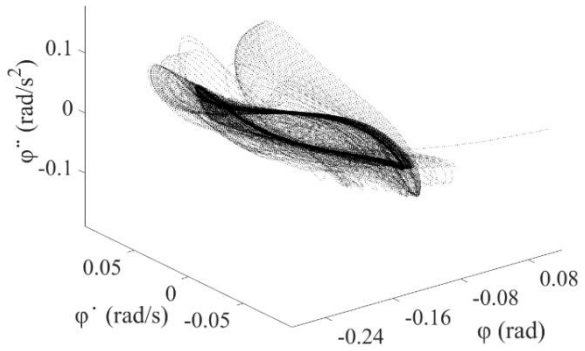

b. Roll angle, Roll acceleration and Roll rate.

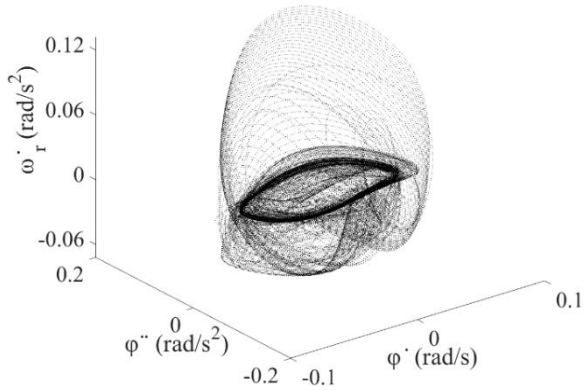

c. Yaw velocity, Roll rate and Roll acceleration

Figure 2. Trajectories of the system

Furthermore, to investigate chaos in the system, bifurcation diagrams are used.

Since the actuator of the closed-loop system is the front active steering, it is necessary to study bifurcation diagrams to find chaos boundaries. Chaotic, quasi-periodic and periodic behavior of the system, with respect to changes in the steering angle are displayed in figure 3.

In figure 3a, as the lateral angle reaches 0.01 rad chaos occurs.

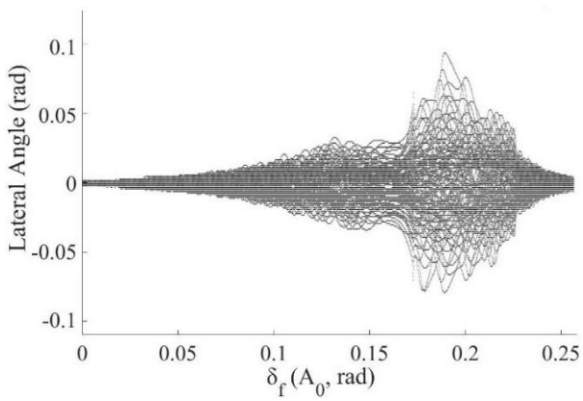

a. Lateral angle

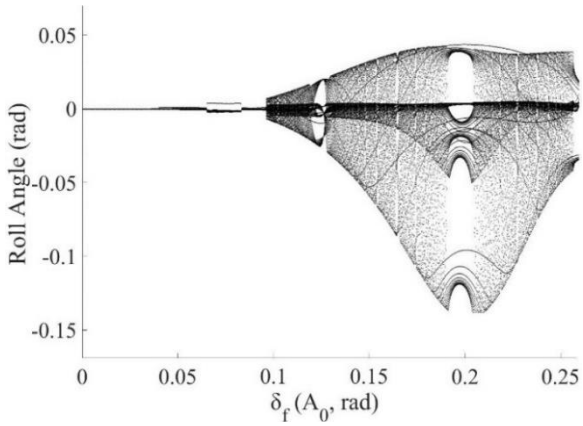

b. Roll angle

Figure 3. Bifurcation diagrams under amplitude changes

According to figure 3b, for $\delta_f > 0.19\,rad/s$ transition to chaos is observed. Bifurcation diagrams in terms of lateral forces on the vehicle axles are presented in figure 4. For $\delta_f > 0.05$ in fig. 4a, and $\delta_f > 0.1$ chaos is obvious.

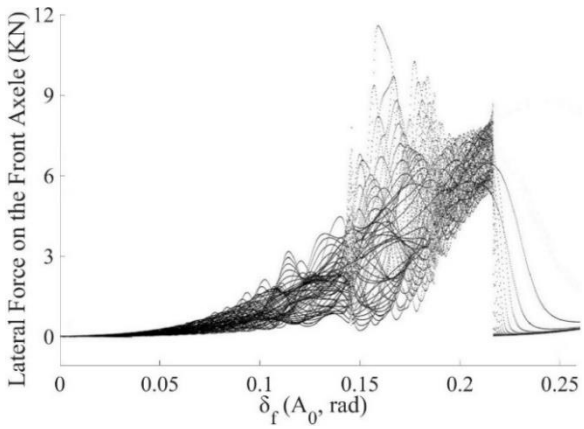

a. front axle

[DOI: 10.22068/ase.2021.602]

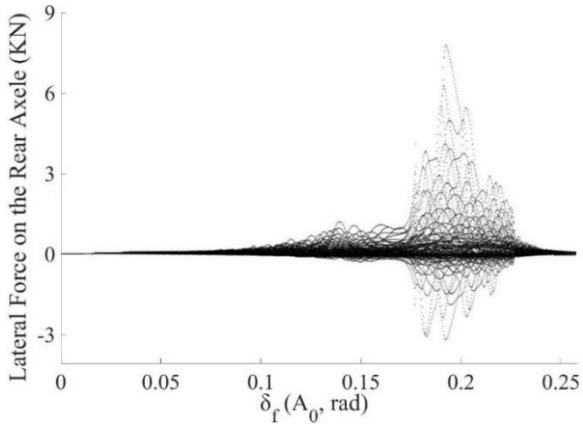

b. rear axle

Figure 4. Bifurcation diagrams for Lateral forces

4. Chaos Control

OGY method is based on the Poincaré map of the system [10]. For this purpose, either linear or nonlinear map is used. In this paper the method is applied to control chaos due to advantages such as robustness and reducing the system order.

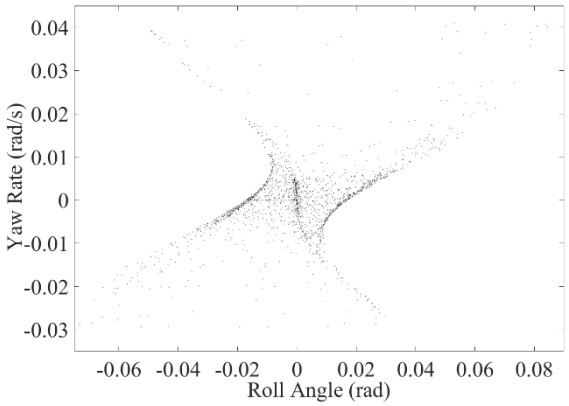

Figure 5. Poincaré Section

4.1. Derivative of Poincaré map

the Poincaré map is derived by means of neuro fuzzy network. To this end, the Poincaré section displayed in Figure 5, which is based on the phase plane trajectory of the system (figure 2c), is chosen to determine the map. This is due to apropos distribution and appropriate quantity of the points in this section.

Moreover, Mamdani type of neuro fuzzy is used to train data and clustering. The general equation is $F(x) = \sum_{i=1}^{n} b_i\, y_i K(x, x_i) + w_0$ which b_i is the bias of the function, w indicates weights and $K(x, x_i)$ is the base function. To reduce errors, sigmoid function is considered for kernel function. 60% of the data are used for training while 20% is for testing and 20% for validating. As a result, Poincare' map is obtained and represents a description for the system.

$$\begin{aligned} Y_{n+1} &= [b2_y] + [Lw_y] \times \{2/(1+\exp(-2 \times \\ &\quad ([b1_y] + [Iw_y] \times [X_n, Y_n]))) - 1\} \\ X_{n+1} &= [b2_x] + [Lw_x] \times \{2/(1+\exp(-2 \times \\ &\quad ([b1_x] + [Iw_x] \times [X_n, Y_n]))) - 1\} \end{aligned} \quad (6)$$

Front steering angle values are used as input in simulating the equations.

4.2. Fuzzy logic controller design on the nonlinear Poincaré map

The block diagram of the closed-loop system is presented in Figure 6.

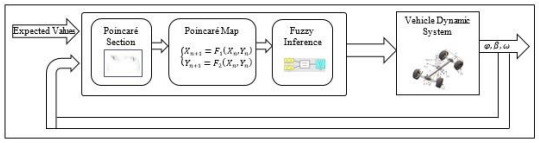

Figure 6. Block diagram of the chaos control system

The deviation between the output and the expected values of the system is used as the input of the fuzzy interface. Adjusting the steering angle leads in stabilizing the irregular lateral movements. The desired values of the system for yaw, roll and sideslip angles, respectively are [8]:

$$\begin{aligned} \beta^* &= \left(l_r/l(1+kv^2)\right. \\ &\quad \left. + l_f m v^2/C_{rl}^2(1+kv^2)\right) \\ \omega^* &= v\delta_f/l(kv^2),\ \varphi^* = 0 \end{aligned} \quad (9)$$

According to figure 6 expected values and feedback values are given a control parameter. As presented in figure 7, due to simple formulas and computational efficiency, Gaussian combination and Gaussian curve membership functions are considered to achieve a smooth control signal. [11].

[DOI: 10.22068/ase.2021.602]

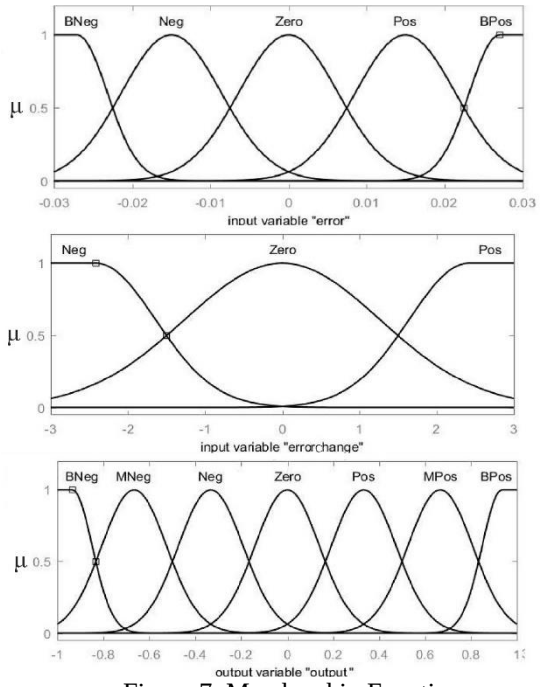

Figure 7. Membership Functions

In fuzzy controller design, the rules for membership functions are listed in Table 2. Input linguistic variables are set in these rules such that positive and Large positive errors are (P, BP), negative and Large negative errors are (N, BN), and for no error, (Zero) is used. (N, Zero, P), indicate negative, zero and positive error changes respectively. For the output, possible modes, including large, medium and small positive control signals are (BP, MP, SP), and (Zero) is used to indicate zero. On the other hand, large, medium and small negative control signals are (BN, MN, SN).

Table 2. Fuzzy Controller Rules

$\dot{e}$ / e	**Big Negative**	**Negative**	**Zero**	**Positive**	**Big Positive**
Negative	Big Negative	Medium Negative	Negative	Zero	Positive
Zero	Medium Negative	Negative	Zero	Positive	Medium Positive
Positive	Negative	Zero	Positive	Medium Positive	Big Positive

4.3. Simulation of feedback chaos Controller

The front steering angle input with frequency of 2.5 Hz held and 0.12 rad is applied to the system. The comparison between the expected conditions and the closed-loop system controlled is shown in Figure 8. According to the figure, in roll, the desired value is zero while the change of the input from front steering angle creates a chaotic situation and the proposed controller, eliminates the chaotic behavior and the system at approximate 0.02 rad angle is stabilized.

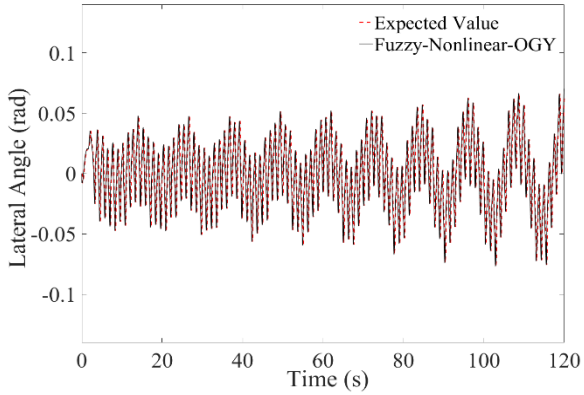

a. Lateral angle

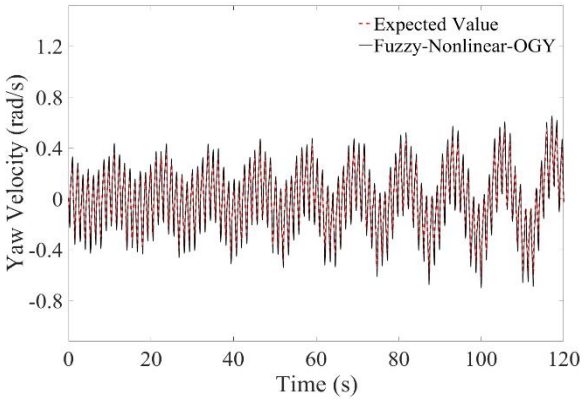

b. Yaw velocity

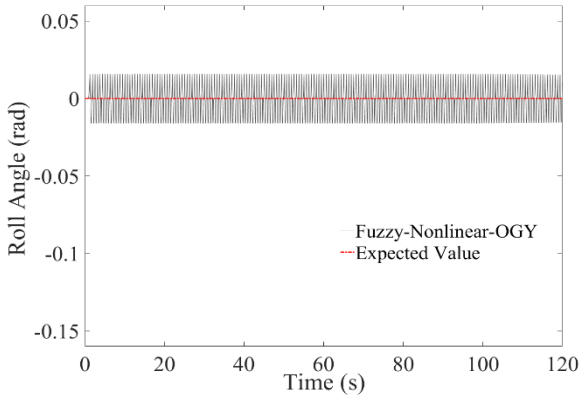

c. Roll angle

Figure 8. Simulation results of closed-loop system

4.4. Analysis of controller performance in different maneuvers

To simulate the acute driving conditions, the input for the front steering angle is considered to be step and sinusoidal. The initial input frequency of the front wheel steering angle was 3 rad/s and the value was held constant at 0.12 rad for step

[DOI: 10.22068/ase.2021.602]

input while sinusoidal input simulated by $i = A \sin \omega t$. Figure 9 presents the simulation results of the closed-loop system for lateral angle, yaw velocity and roll angle, respectively. Step input is applied to the system.

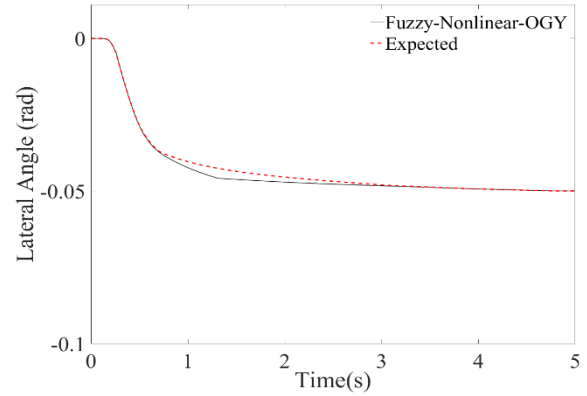

a. Lateral angle

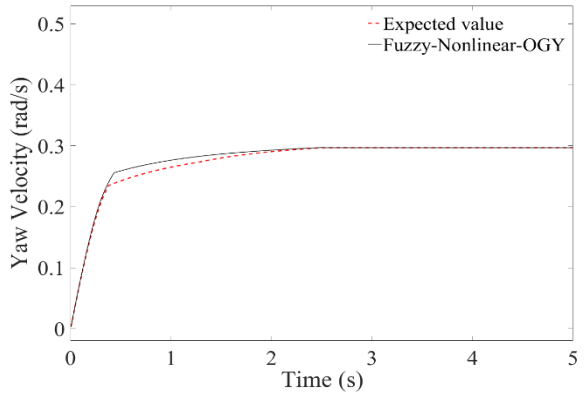

b. Yaw velocity.

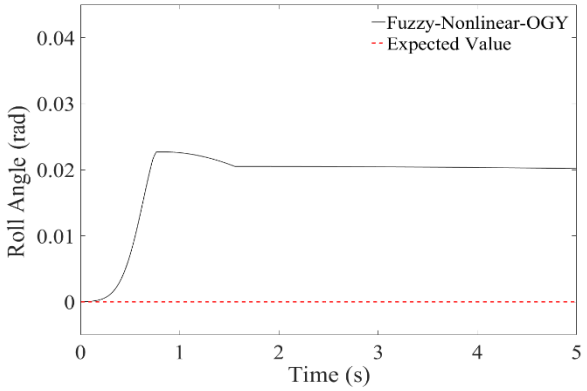

c. Roll angle

Figure 9. Simulation results for Step Input

For the lateral angle and yaw velocity shown in Figure 10, the controlled results correspond to the expected values. At the roll angle, due to the continuous oscillating input of the steering wheel, the controller has limited the roll angle deviation of the system to $[-0.02, 0.02]$. Also for step inputs, results of the roll angle are limited to 0.02.

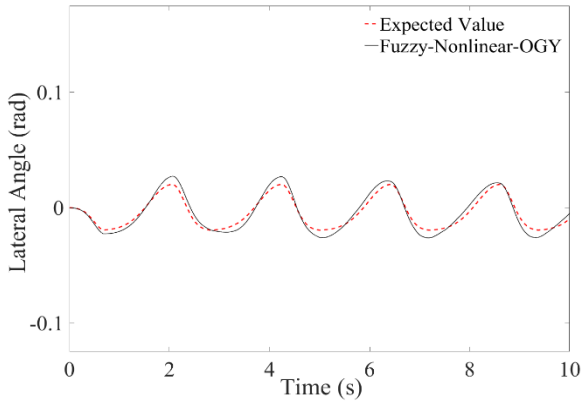

a. Lateral angle

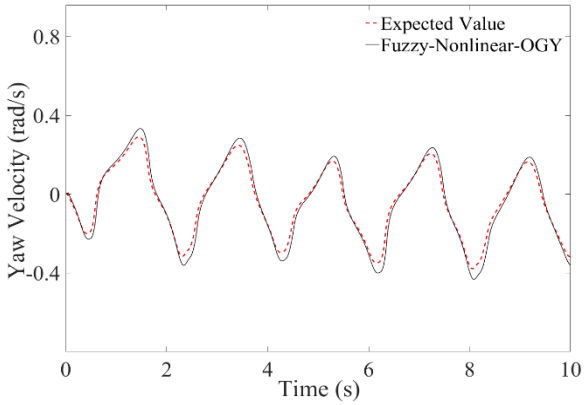

b. Yaw velocity.

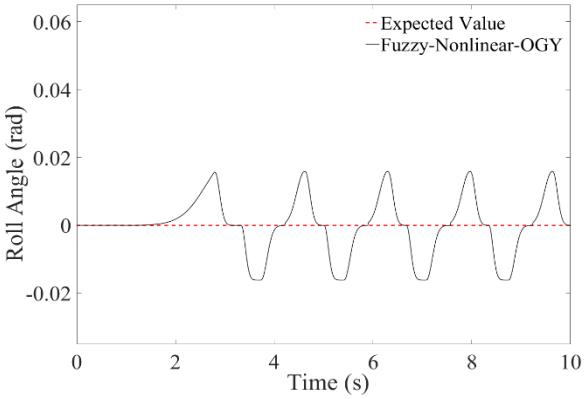

c. Roll angle

Figure 10. Simulation results for oscillating Input

The controller holds the converges the system to the desired conditions for the lateral angle and yaw velocity. The control signal is presented in figure 12. According to the figure, the fuzzy-nonlinear OGY controller, has a low energy consumption.

[DOI: 10.22068/ase.2021.602]

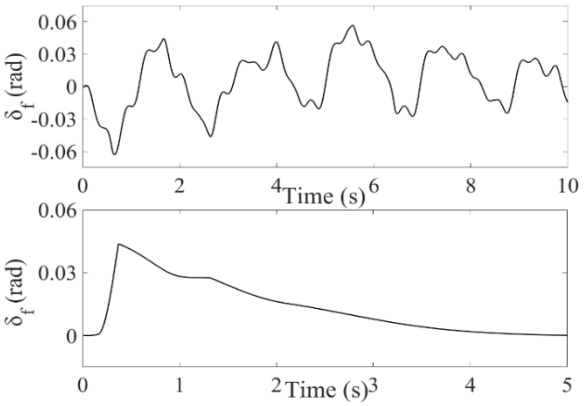

Figure 12. Time series responses of fuzzy-nonlinear OGY controller signal for sinusoidal and step input

5. Conclusion

In this paper, lateral dynamic system of a vehicle is modeled and chaotic behavior of the system is investigated by the use of Lyapunov exponent and bifurcation diagrams. Thus, different aspects of chaos are studied. Poincaré map of the system is estimated by means of neuro fuzzy method. Consequently, the order of the system is reduced. To eliminate the chaos and stabilize the system, a novel nonlinear fuzzy-OGY controller is designed. Step and sinusoidal inputs are applied to the closed-loop system.

According to the results, in step inputs, 14% in lateral angle and 26% in yaw velocity reduced the time to reach the expected values and improve the roll angle error by 12%. In oscillating inputs, this method has a better control compared to the adaptive sliding mode, 12% lateral angle, 10% yaw velocity and 2% roll angle. The accuracy and pace of the novel controller with low energy consumption, control the chaotic behavior of the system, meanwhile the vehicle model is devoid of instability leading to loss of control, which confirms the Fuzzy nonlinear controller based on the Poincaré nonlinear map method.

Notion:

$C_{sl}, C_{sr}\ (Ns\ /\ m)$	linear damping coefficients of the left and right suspension
$C_{l1}, C_{r1}\ (Ns^2/m^3)$	nonlinear stiffness coefficients of the left, right suspension
$f_0\ (Hz)$	lower cut-off frequency
$F_{yf}, F_{yr}\ (N)$	lateral forces on front, rear axles
$F_{sl}, F_{sr}\ (N)$	supporting forces of the left, right suspension elements
$G_0\ (m^3)$	road roughness coefficient
$h\ (m)$	distance from the center of mass to the roll axis
$I_z, I_{sx}\ (kg\ m^2)$	moment of inertia around axle Z and X
$K_l, K_r\ (N\ /\ m)$	linear stiffness coefficients of the left, right suspension
$K_{l2}, K_{r2}\ (N\ /\ m)$	nonlinear stiffness coefficients of the left, right suspension
$l_f, l_r\ (m)$	distance from the center of mass to the front, right axles
$m\ (kg)$	total vehicle mass
$m_s(kg)$	vehicle suspended mass
$q_l, q_r\ (m)$	road surface inputs at the left and right sides
$T\ (m)$	distance between the left and right wheels
$v\ (m/s)$	longitudinal velocity of the vehicle
w_i	zero-mean Gaussian white noise
$z_l, z_r\ (m)$	relative displacement between the upper retaining points of the left and right suspension and the road surface
$\alpha_f, \alpha_r\ (rad)$	Front and right wheel sideslip angles
$\beta\ (rad)$	sideslip angle
$\delta_f\ (rad)$	front steering angle
$\varphi(rad)$	roll angle
$\omega_r\ (rad/s)$	yaw velocity

***References*:**

[1] E. Ott, C. Grebogi, and J. A. Yorke, "Controlling chaos," *Phys. Rev. Lett.*, vol. 64, no. 11, pp. 1196–1199, 1990, doi: 10.1103/PhysRevLett.64.1196.

[2] S. M. Abtahi and S. H. Sadati, "Chaos control in attitude dynamics of a gyrostat satellite based on linearised Poincare' map estimation by support vector machine," *Proc. Inst. Mech. Eng. Part K J. Multi-body Dyn.*, vol. 227, no. 3, pp. 302–312, 2013, doi: 10.1177/1464419313490681.

[3] S. M. Abtahi, S. H. Sadati, and H. Salarieh, "NONLINEAR ANALYSIS AND ATTITUDE CONTROL OF A GYROSTAT SATELLITE WITH CHAOTIC DYNAMICS USING," vol. 18, no. 6, pp. 1–11, 2016, doi: 10.1002/asjc.1278.

[4] S. M. Abtahi, "Chaotic study and chaos control in a half-vehicle model with semi-active

[DOI: 10.22068/ase.2021.602]

suspension using discrete optimal Ott-Grebogi-Yorke method," in *Proceedings of the Institution of Mechanical Engineers, Part K: Journal of Multi-body Dynamics*, 2017, vol. 231, no. 1, pp. 148–155, doi: 10.1177/1464419316655515.

[5] H. Mirzaeinejad, M. Mirzaei, and S. Rafatnia, "A novel technique for optimal integration of active steering and differential braking with estimation to improve vehicle directional stability," *ISA Trans.*, vol. 80, pp. 513–527, 2018, doi: 10.1016/j.isatra.2018.05.019.

[6] J. Cho and K. Huh, "Active Front Steering for Driver's Steering Comfort and Vehicle Driving Stability," *Int. J. Automot. Technol.*, vol. 20, no. 3, pp. 589–596, 2019, doi: 10.1007/s12239-019-0056-1.

[7] R. Dehghani, H. M. Khanlo, and J. Fakhraei, "Active chaos control of a heavy articulated vehicle equipped with magnetorheological dampers," *Nonlinear Dyn.*, vol. 87, no. 3, pp. 1923–1942, 2017, doi: 10.1007/s11071-016-3163-9.

[8] W. Chen, R. Zhang, L. Zhao, H. Wang, and Z. Wei, "Control of chaos in vehicle lateral motion using the sliding mode variable structure control," *Proc. Inst. Mech. Eng. Part D J. Automob. Eng.*, vol. 233, no. 4, pp. 776–789, 2019, doi: 10.1177/0954407017753529.

[9] S. Jerath and S. Gurav, "Road surface roughness generation by power spectral density in bridge design," in *Proceedings of the 2008 Structures Congress - Structures Congress 2008: Crossing the Borders*, 2008, vol. 314, no. October 2008, doi: 10.1061/41016(314)312.

[10] S. M. M. Kashani, H. Salarieh, and G. Vossoughi, "Control of nonlinear systems on Poincaré section via quasi-sliding mode method," *Commun. Nonlinear Sci. Numer. Simul.*, vol. 14, no. 3, pp. 645–654, 2009, doi: 10.1016/j.cnsns.2007.11.007.

[11] B. Li and F. Yu, "Design of a vehicle lateral stability control system via a fuzzy logic control approach," *Proc. Inst. Mech. Eng. Part D J. Automob. Eng.*, vol. 224, no. 3, pp. 313–326, 2010, doi: 10.1243/09544070JAUTO1279.

[DOI: 10.22068/ase.2021.602]